Electronic Supplementary Information:

Benchmarking atomically defined AFM tips for chemical-selective imaging

Bertram Schulze Lammers[a,b] Damla Yesilpinar[a,b] Alexander Timmer[b]
Zhixin Hu*[c] Wei Ji[d] Saeed Amirjalayer[1,2,5] Harald Fuchs[a,b]
Harry Mönig*[a,b]

[a]Physikalisches Institut, Westfälische Wilhelms-Universität, 48149 Münster, Germany
[b]Center for Nanotechnology, 48149 Münster, Germany
[c]Center for Quantum Joint Studies and Department of Physics, Tianjin University, Tianjin, China
[d]Department of Physics and Beijing Key Laboratory of Optoelectronic Functional Materials & Micro-Nano Devices, Renmin University of China, Beijing, China
[e]Center for Multiscale Theory and Computation, 48149 Münster, Germany

***Email:** harry.moenig@uni-muenster.de or zhixin.hu@tju.edu.cn

1 Methods

Sample Preparation. The Cu(110) single crystal were cleaned by cycles of Ar^+ puttering and subsequent annealing up to 600 K, each for 10 min. After the final annealing we waited for roughly 5 min to reach a sample temperature of 450 to 500 K. At this temperature molecular O_2 is dosed with $2 \cdot 10^{-8}$ mbar for 10 to 15 s to induce the (2×1)O-reconstructed oxide stripes. Sample temperature and amount of O_2 dosing influence the widths of the reconstruction.

Tip Preparation. The general tip forming processes are performed and controlled in STM mode with a set-point of 0.1 mV and 50 pA. The basis of each tip is a stable and sharp copper tip, which is created by voltage pulses and indentations into the bare Cu(110) areas.

The Xe-tip is formed by picking up a Xe atom from the surface. 6 to 12 L of xenon gas are dosed on the cold partially oxidized Cu(110) sample, placed at 10 K inside the microscope. This dosage leads to 1-4 atomic chains at the boundaries of the oxide stripes. Vertical approaching on one Xe atom by 3 to 4 Å induces picking it up, which is confirmed by a missing Xe atom and a sharper contrast in subsequent STM imaging.

By dosing 0.9 L of CO gas instead, single CO molecules can be observed as dark spots on the bare Cu(110) areas. In STM mode (0.1 mV, 50 pA) 3-5 neighboring CO molecules are selected on an area, where the molecules can be manipulated towards each other. When the height for the manipulation is reduced by 1 to 3 Å, a CO molecule can be picked up spontaneously, at this point the contrast changes and the former dark appearance of the CO molecules on the surface exhibit a bright center [1].

To obtain a covalently bound CuOx-tip, a sharp Cu-tip is indented by about 1 to 8 Å into the oxide stripes. This produces a cluster of oxygen and copper atoms at the apex, which is shaped by further small indentation until a symmetric and clear contrast is observed. By AFM imaging above an oxide stripe a specific contrast serves as a fingerprint for the CuOx-tip and confirms its oxygen-down configuration [2,3]. Potential asymmetries of a CuOx apex can be detected by contrast analysis in the regime where repulsive forces start dominating. Some examples allowing to identify tip asymmetry are given in Supplementary Fig. S1. Further tip forming procedures involving indentations of up to 40 Å with an applied bias voltage of 4 to 8 V might be required to achieve a symmetric and stable CuOx-tip. Estimating the statistics of success starting with clean conditions of sample and tip apex, one out of 10 to 20 leads to a stable and symmetric CuOx-tip apex.

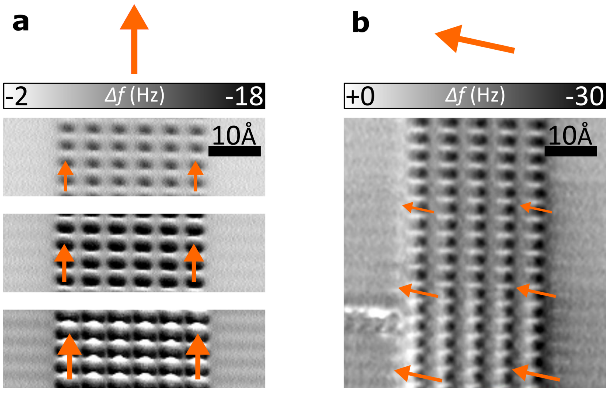

Supplementary Figure S1: Examples for the contrast obtained with asymmetric CuOx-tips. The orange arrows mark the orientation of the tip asymmetry. It is emphasized at reduced tip-sample distances where repulsive forces start dominate. (a) Asymmetry is parallel to the oxide stripe for three different tip-sample distances. Tip asymmetry most distinct at reduced tip sample distance (bottom panel). (b) Asymmetry is almost perpendicular to the oxide stripe.

Computational details. Density functional theory calculations were conducted with the projector augmented wave method [4,5] as implemented in Vienna ab initio simulation package (VASP) [6]. Energy cutoff for the plane wave basis was set to 400 eV. Van-der-Waals interaction [7] was described by the vdW-DF method with optB86b exchange functional [8]. The substrate was modeled with four layers of copper atoms, separated by 30 Å vacuum space on the Z-direction. Two added rows with alternating copper and oxygen atoms were placed on the surface. Only the gamma point is used to sample the first Brillouin zone of the unit cell. Tips were formed by around twenty atoms. All atoms except for bottom two layers were fully relaxed until residual forces were less than 0.02 eV/Å. To quantitatively determine the spring constants, we analyzed the vibrational modes of the tips and derived the force constants from the corresponding frequencies (Supplementary Fig. S3). For the force curve calculation, only the terminating 4-6 atoms from the tip were relaxed. Forces were calculated from the first derivative of internal energy. The tip height Z is defined as the vertical distance between the initial position of tip termination and the AR-O atom.

2 Contrast effects caused by tip flexibility

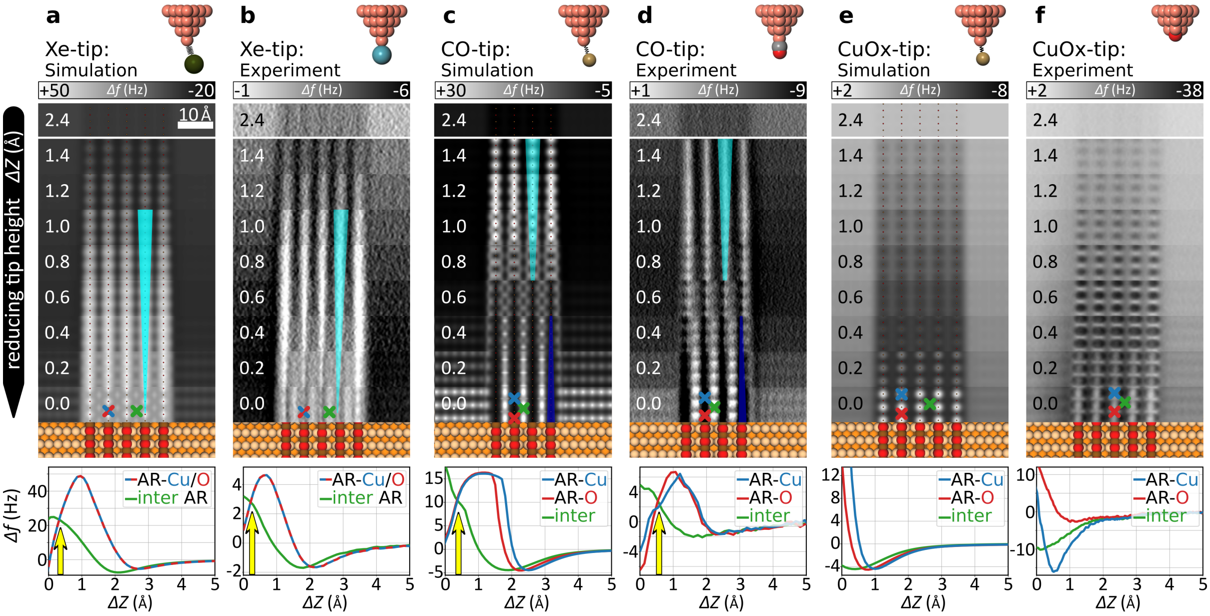

Supplementary Figure S2: Tip flexibility effects in simulations and experiments. (a) Simulation for a Xe-tip ($k_\mathrm{h} = 8.1\,\mathrm{N/m}$; $k_\mathrm{v} = 10.3\,\mathrm{N/m}$). (b) Experimental data for the Xe-tip re-plotted from Fig. 2b (main manuscript). (c) Simulation for a CO-tip ($k_\mathrm{h} = 1.7\,\mathrm{N/m}$; $k_\mathrm{v} = 326.9\,\mathrm{N/m}$). (d) Experimental data for the CO-tip re-plotted from Fig. 2c (main manuscript). (e) Simulation for a CuOx-tip ($k_\mathrm{h} = 161.97\,\mathrm{N/m}$; $k_\mathrm{v} = 271.1\,\mathrm{N/m}$). (f) Experimental data for the CuOx-tip re-plotted from Fig. 2d (main manuscript). The sharpening effect of the flexible Xe- and CO-tips is highlighted by the light blue colored tapering lines and the inverse sharpening (widening) in dark blue. The data is supported by background-subtracted Δf-spectra, whose positions are marked by color-coded crosses. The background spectra were taken on the bare Cu(110) area and the yellow arrows mark the specific crossing points of spectra according to a contrast inversion in the repulsive force regime.

For the contrast simulations in Supplementary Fig. S2 an effective tip charge of $-0.05\,\mathrm{e}$ and DFT-calculated spring constants summarized in Supplementary Fig. S3 are considered. The simulations can reproduce the main contrast features of the flexible Xe- and CO-tip (Supplementary Fig. S2a-d). In agreement with previous studies[9,10], an artificial sharpening effect occurs at tip heights $\Delta Z < 1.0\,\mathrm{Å}$ for the Xe-tip and at $\Delta Z < 1.4\,\mathrm{Å}$ for the CO-tip in the simulation and in the experimental data (light blue tapering lines). It is interesting to note that we find also a reversed effect for the CO-tip, where with decreasing ΔZ the dark trenches above the added rows (ARs) become broader. This evolution is found in both, simulation and experiment at tip-heights below the point of contrast inversion (Supplementary Fig. S2).

At the lower end of the sharpening, the ARs remain as thin lines, which is slightly more pronounced in the experimental data. The last Xe-tip frames show that the inter sites become increasingly brighter, whereby the contrast is inverted at this point. For the CO-tip the contrast inversion occurs at $\Delta Z \approx 0.6$ Å, which results in a dark appearance of the ARs and atomically corrugated bright features on the inter sites in simulation and experiment. As stated in the main manuscript, by comparing the simulated and experimental Δf-spectra, the location of the bright features can be assigned to the inter sites between two AR-O atoms. However, it should be noted that this holds only for the case of the CO-tip. The data of for the Xe-tip do not allow such an identification of atomic sites.

By comparing the experimental and simulated Δf-spectra for the CO- and Xe-tip, a good qualitative agreement is found. In particular, we find the typical dip-hump appearance indicative for pronounced tip bending[11]. Furthermore, this holds for the crossing points in the spectra marking the contrast inversion.

In case of the simulation for the CuOx-tip, the contrast on the AR-Cu sites reasonably reproduces the experimental data (Supplementary Fig. S2e,f). In particular, by reducing the tip height, the AR-Cu sites become darker down to $\Delta Z \approx 0.4$ Å. Here, a weak bright feature appears in the center of the AR-Cu atoms. This feature becomes larger and brighter for further reducing ΔZ, until it dominates the overall appearance at $\Delta Z = 0.0$ Å in the simulation as well as in the experiment. However, in contrast to the AR-Cu sites, the bright horizontal signature of the AR-O atoms in experiment at tip heights $\Delta Z < 0.6$ Å cannot be reproduced by the simulation. Accordingly, the Δf-spectra on the AR-O site differ significantly (red spectra in Supplementary Fig. S2e,f). In the simulated spectrum a clear minimum is observed, in contrast to the marginal minimum shown in the experimental spectrum. In general, the used model mainly reflects the influence of tip flexibility, but it does not consider the chemical interaction, hence it cannot reproduce the atomic selectivity.

3 Simulations based on density functional theory

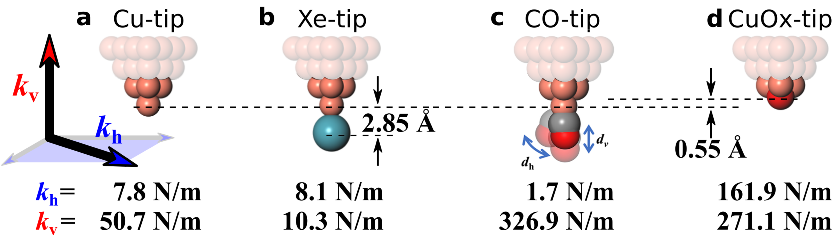

Supplementary Figure S3: Tip models for quantifying horizontal and vertical spring constants by DFT simulations. The tip bases are represented by a tetrahedral Cu_{20} cluster, while the upper two layers were kept fixed in the models. For the metallic Cu-tip, the lowest copper atom represents the terminating atom, where for the Xe- and CO-tip an additional atom or molecule is attached. By replacing the lowest copper atom with a strongly bound oxygen atom, the CuOx-tip is formed. Here, the terminating oxygen atom is 0.55 Å closer to the upper Cu-layer. For the Cu-, Xe-, and CuOx-tip, horizontal and vertical spring constants (k_h, k_v) were determined by analyzing the vibrational frequencies of the terminating atom. For the CO-tip, C and O atoms were displaced together since the C-O bond is much stronger than the C-Cu bond (horizontal and vertical displacement d_h and d_v as indicated). The vibrational coupling with non-adjacent copper atoms is neglected. The Xe-Cu distance in the Xe-tip is 2.85 Å, indicating a van der Waals interaction regime. The slope of potential energy versus Xe-Cu distance is so flat that force constants are similar along vertical and horizontal directions.

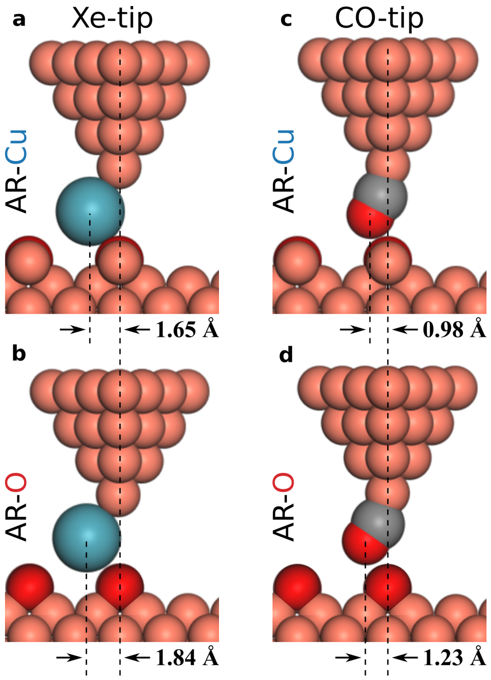

Supplementary Figure S4: The deflection of flexible tips on the AR-Cu and AR-O site is simulated by DFT. (a) and (b): Tilted Xe-tip. (c) and (d): Tilted CO-tip. All simulations refer to the tip height $Z = 2.4\,\text{Å}$ between the center of AR-O atom and the initial position of the tip-terminating atom. Surface atoms are fixed during the calculations. For both tips the repulsion on the AR-O site is stronger than on the AR-Cu site. The size of the terminating atom causes larger deflections for the Xe-tip compared to the CO-tip.

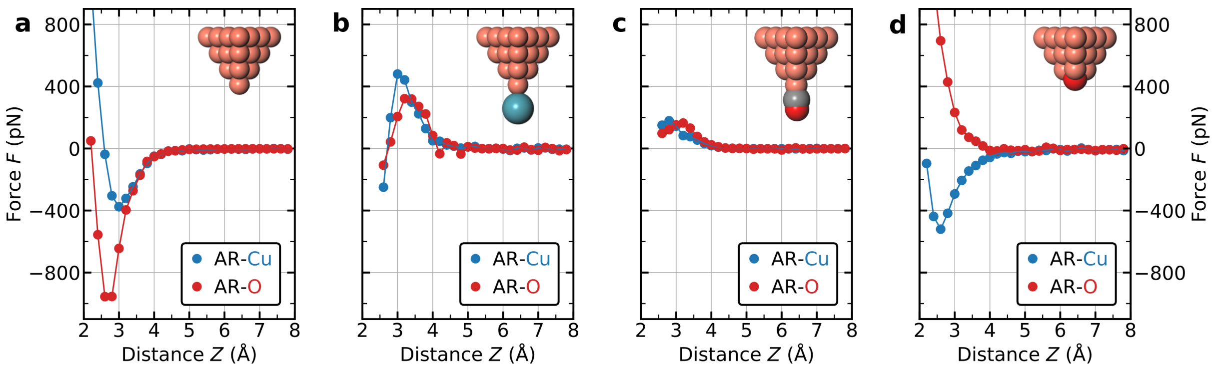

Supplementary Figure S5: DFT-derived force spectra without van-der-Waals contributions. The van-der-Waals (vdW) component is subtracted to focus on the chemical reactivity of the four different tip terminations: (a) Cu-tip; (b) Xe-tip; (c) CO-tip; (d) CuOx-tip. Devoid of vdW-attraction, only the metallic Cu-tip in (a) shows strong attractions on *both* added row sites (AR-Cu and AR-O), which reflects its strong chemical reactivity. In contrast, the passivated Xe- and CO-tips, in (b) and (c), do not exhibit any attractive chemical interaction; in accordance to their inert probe particles. Between 3.0 Å and 3.5 Å the force curves in (b) and (c) have kinks, which is caused by the deflection of the terminating probe particles (Supplementary Fig. S4). For the CuOx-tip in (d) the AR-Cu site induces a strong attraction around $Z = 2.6$ Å. In contrast, the AR-O site does not exhibit chemical attractive interaction, but it shows a strong repulsion at reduced Z values.

References (Electronic Supplementary Information)

[1] L. Gross, F. Mohn, N. Moll, P. Liljeroth, and G. Meyer *Science*, vol. 325, no. 5944, pp. 1110–1114, 2009.

[2] H. Mönig, D. R. Hermoso, O. Díaz Arado, M. Todorović, A. Timmer, S. Schüer, G. Langewisch, R. Pérez, and H. Fuchs *ACS Nano*, vol. 10, no. 1, pp. 1201–1209, 2016.

[3] H. Mönig, S. Amirjalayer, A. Timmer, Z. Hu, L. Liu, O. Díaz Arado, M. Cnudde, C. A. Strassert, W. Ji, M. Rohlfing, and H. Fuchs *Nat. Nanotechnol.*, vol. 13, no. 5, pp. 371–375, 2018.

[4] P. E. Blöchl *Phys. Rev. B*, vol. 50, pp. 17953–17979, 1994.

[5] G. Kresse and D. Joubert *Phys. Rev. B*, vol. 59, pp. 1758–1775, 1999.

[6] G. Kresse and J. Furthmüller *Phys. Rev. B*, vol. 54, pp. 11169–11186, 1996.

[7] M. Dion, H. Rydberg, E. Schröder, D. C. Langreth, and B. I. Lundqvist *Phys. Rev. Lett.*, vol. 92, p. 246401, 2004.

[8] J. Klimeš, D. R. Bowler, and A. Michaelides *J. Phys. Condens. Matter*, vol. 22, no. 2, p. 022201, 2009.

[9] L. Gross, F. Mohn, N. Moll, B. Schuler, A. Criado, E. Guitián, D. Peña, A. Gourdon, and G. Meyer *Science*, vol. 337, no. 6100, pp. 1326–1329, 2012.

[10] P. Hapala, G. Kichin, C. Wagner, F. S. Tautz, R. Temirov, and P. Jelínek *Phys. Rev. B*, vol. 90, p. 085421, 2014.

[11] N. Néel and J. Kröger *Nano Lett.*, vol. 21, no. 5, pp. 2318–2323, 2021.